JACS
JOURNAL OF THE AMERICAN CHEMICAL SOCIETY

Article

pubs.acs.org/JACS

Conformations of Prolyl−Peptide Bonds in the Bradykinin 1−5 Fragment in Solution and in the Gas Phase

Liudmila Voronina,[†] Antoine Masson,[†,∥] Michael Kamrath,[†] Franziska Schubert,[‡] David Clemmer,[§] Carsten Baldauf,*[,‡] and Thomas Rizzo*[,†]

[†]Laboratoire de Chimie Physique Moléculaire, École Polytechnique Fédérale de Lausanne, EPFL SB ISIC LCPM, Station 6, CH-1015 Lausanne, Switzerland

[‡]Fritz-Haber-Institut der Max-Planck-Gesellschaft, D-14195 Berlin, Germany

[§]Department of Chemistry, Indiana University, Bloomington, Indiana 47405, United States

Supporting Information

ABSTRACT: The dynamic nature of intrinsically disordered peptides makes them a challenge to characterize by solution-phase techniques. In order to gain insight into the relation between the disordered state and the environment, we explore the conformational space of the N-terminal 1−5 fragment of bradykinin ($BK[1-5]^{2+}$) in the gas phase by combining drift tube ion mobility, cold-ion spectroscopy, and first-principles simulations. The ion-mobility distribution of $BK[1-5]^{2+}$ consists of two well-separated peaks. We demonstrate that the conformations within the peak with larger cross-section are kinetically trapped, while the more compact peak contains low-energy structures. This is a result of *cis*−*trans* isomerization of the two prolyl-peptide bonds in $BK[1-5]^{2+}$. Density-functional theory calculations reveal that the compact structures have two very different geometries with *cis*−*trans* and *trans*−*cis* backbone conformations. Using the experimental CCSs to guide the conformational search, we find that the kinetically trapped species have a *trans*−*trans* configuration. This is consistent with NMR measurements performed in a solution, which show that 82% of the molecules adopt a *trans*−*trans* configuration and behave as a random coil.

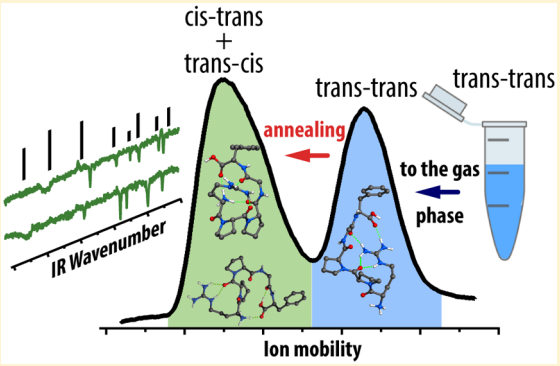

1. INTRODUCTION

Information about the structure and dynamics of proteins and peptides is crucial for understanding their physiological function and hence essential for diagnostics and drug design.[1,2]

X-ray crystallography and NMR spectroscopy can often successfully determine the structure of biomolecules when they adopt well-defined secondary structures.[3] However, in the case of intrinsically disordered peptides, NMR spectra often represent an average over an ensemble of different conformations. Moreover, crystallization for X-ray measurements is often not possible due to the highly dynamic character of the disordered states.[4−6] Many questions thus remain open regarding the nature of intrinsically disordered peptides: Does their flexibility come from solution conditions? What are the main factors contributing to the rapid structural changes? How many well-defined conformers are converting among each other? How does recognition by receptors or membrane insertion happen from a structural perspective?[1,7,8]

One of the most well-studied representatives of partially disordered peptides is the nonapeptide bradykinin (BK), which plays a regulatory role in the cardiovascular and nervous systems and is a key reporter molecule in inflammation and pain.[9] It was shown that in pure aqueous solution the entire peptide exhibits many conformational states rather than a single, well-defined secondary structure.[10] In an aprotic solvent or upon interaction with lipid vesicles, however, residues 6−9 of the C-terminus of BK adopt β-turn-like structures, while residues 1−5 remain "disordered".[11,12] A similar observation was made by Glaubitz and co-workers for BK bound to the human G-protein coupled receptor B2, which was investigated by solid-state NMR: residues 6−8 (Ser-Pro-Phe) appear ordered, while residues 1−5 exhibit a high structural flexibility.[13]

One potential source of conformational heterogeneity of BK, as well as of many other peptides, is proline *cis*−*trans* isomerization,[14] as the BK sequence contains proline in positions 2, 3, and 7. However, most studies performed by NMR find that in the major conformer of BK all prolyl-peptide bonds are in the *trans* conformation, both in free peptide and when bound to a receptor.[11−13,15−18] In general, *cis*−*trans* isomerization of the X-Pro bond is an important biological process; peptidyl-prolyl *cis*−*trans* isomerases (PPIs), which catalyze conversion between *cis* and *trans* conformations in

Received: May 3, 2016
Published: July 1, 2016

DOI: 10.1021/jacs.6b04550
J. Am. Chem. Soc. 2016, 138, 9224−9233

peptides and proteins, are known to play key roles in the functioning of living cells.[19,20] Of the three known families of PPIs, a member of the cyclophilin family, PPIA, can be found in the extracellular medium, where BK is acting, and is linked to, for example, inflammation scenarios.[21,22] Studies of the substrate specificity of PPIA shows activity even for the Pro-Pro prolyl−peptide bond, but it is not known if BK is a substrate for PPIA in a particular physiological process.[23] Besides this, the *cis*−*trans* states of prolyl-peptide bonds can be influenced by interactions with cations[24,25] or by stretching forces along the peptide backbone, which are induced electrostatically[26] or mechanically.[27−29]

A powerful way to obtain insight into the nature of intrinsically disordered peptides is to study them in the gas phase in the absence of solvent.[30−39] For instance, using ion mobility spectrometry (IMS), Bowers and co-workers investigated BK in its singly protonated and sodiated forms. They observed only one peak, invariant of the charge carrier or the temperature.[40] Clemmer's group has shown that the collisional cross-section (CCS) distribution of triply protonated BK produced via ESI demonstrates the presence of at least three major conformational families,[41] which were attributed to different *cis*−*trans* isomerization states of the prolyl-peptide bonds.[42] Although much insight can be gained from IMS data, an unambiguous assignment of conformers is not possible, since ion mobility provides only an average CCS for a conformational family in the gas phase.[43] Instead, a single IMS peak may contain several distinct conformational families with the same CCS.

The expected distribution of structures produced by electrospray is a mixture of low-energy gas-phase conformers and higher energy structures that are kinetically trapped, with barriers on the potential-energy surface (PES) that prevent isomerization.[44−51] These latter structures are particularly important, as they retain information on the conformation of the molecule in solution. In case of proline *cis*−*trans* isomerization, the energy barrier can be high enough (20−50 kJ/mol)[46] to expect solution-phase isomers to be preserved as metastable, kinetically trapped species. Detailed understanding of these kinetically trapped conformations would allow one to connect information obtained from solution-phase and gas-phase techniques. The low-energy gas-phase conformers, on the other hand, may exemplify possible structure alternation upon change of environmental condition as, for example, during membrane insertion. Vacuum can be understood as an extreme case of an aprotic nonpolar solvent lacking intermolecular interactions. Membranes are generally seen as structure-inducing media, and a question was recently raised if molecular disorder is possible there.[52] Detailed conformational studies in the gas phase might shed light on this question.

In this work, we focus on the 1−5 fragment of BK (Figure 1), which is metabolically stable[53] and was shown to inhibit the enzymatic activity of thrombin.[54−56] Russell and co-workers[57] have investigated the 1+ charge state of this molecule by IMS and H/D exchange after matrix-assisted laser desorption ionization (MALDI). Three distinct structural forms were found, exhibiting a relative abundance dependent on the composition of the solvent. The extended form was observed when a high water concentration was used.

We investigate the conformational preferences of BK[1−5] in the +2 charge state by combining drift tube ion mobility with cryogenic-ion spectroscopy and quantum-chemical calculations. Experimental constraints are used to guide the first-principles

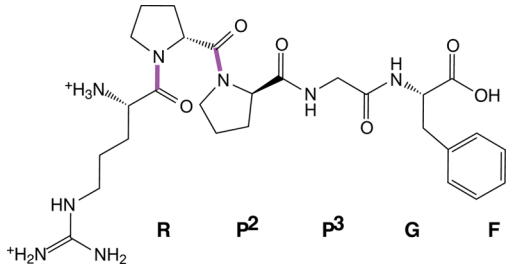

Figure 1. Chemical structure of doubly protonated bradykinin residues 1−5 (BK[1−5]$^{2+}$). The two positive charges are located at the side chain of the arginine residue and at the N-terminus. The bonds around which the *cis*−*trans* isomerization can occur are highlighted.

structure search and allow us to identify not only the thermodynamically stable low-energy conformers, but also those that are kinetically trapped. We show that *cis*−*trans* isomerization of BK[1−5] indeed plays a key role in forming distinct conformational families. We identify the kinetically trapped structures and show that they have a direct relationship to those observed by NMR in solution.

2. EXPERIMENTAL AND COMPUTATIONAL APPROACH

Bradykinin[1−5] (RPPGF, trifluoroacetate salt, Bachem) was purchased and used without further purification. Peptide solutions were prepared in a 49:49:2 mixture of water/methanol/acetic acid with a peptide concentration of 50 μM. In the 2+ protonation state, the extra protons are believed to reside on the arginine side chain and on the N-terminal amine.

The experimental part of this work is performed using two home-built, cold-ion spectrometers, both of which are described in detail elsewhere.[58,59] We briefly highlight their salient features below.

2.1. Ion Mobility Spectrometry Coupled with Cryogenic Ion Spectroscopy. We have constructed an instrument (referred to as the IMS-CIS instrument) that combines a linear IMS drift tube with a cold-ion trap and a time-of-flight mass spectrometer for measuring collisional cross-section distributions of a molecule of interest and vibrational spectra of mobility-selected ions.[59] Ions are generated by electrospray and separated according to their collisional cross section in a 2 m long drift tube, developed in the group of Clemmer[60] and incorporated into this instrument without modification. Stand-alone collisional cross section distributions are measured at the end of the drift tube using a channeltron detector. The drift tube can be operated in two modes: as a single 2 m long drift tube or as a tandem IMS-IMS instrument. In the latter mode, we preselect a conformational family of interest in the first half of the drift tube with an ion gate, collisionally activate it in a controlled way, and observe its drift using the second half of the drift tube. Any changes in conformation upon activation manifest themselves in the latter drift-time distribution.

To perform spectroscopic studies of mobility-selected peptide ions, the ion gate at the end of the drift tube is opened for 80 μs so that only those within a predefined range of collisional cross sections pass through and continue to a planar ion trap where they are cooled down to ∼10 K by collisions with hydrogen. Here the ions are tagged with H_2 reporter molecules and interrogated with an infrared laser. Absorption of an infrared photon leads to evaporation of hydrogen and decreases the number of tagged species. The spectrum can thus be recorded by monitoring the number of tagged molecules in the time-of-flight MS as a function of the laser wavelength.[61]

2.2. Conformer-Selective Cold Ion Spectroscopy. Using a separate instrument[58] (referred to as the CIS instrument), we have the ability to separate conformers using IR-UV double-resonance[62] in a cryogenic octopole ion trap and thus obtain vibrational spectra for each of them. The ions are produced by a nanospray source, and after passing through a metal capillary they are injected into an ion funnel. Some collisional activation of the ions invariably occurs at the end of

DOI: 10.1021/jacs.6b04550
J. Am. Chem. Soc. 2016, 138, 9224−9233

the funnel where the diameter of the electrodes is smallest.[63] After being extracted from the funnel, the ions are prestored in a room-temperature hexapole ion trap for 70 ms, mass-selected by a quadrupole mass-filter, and then guided into a cold (4 K) octopole ion trap, where they are cooled by collisions with helium. A UV laser pulse promotes the trapped ions to the first electronically excited state, and since the excitation energy is above the dissociation threshold, some of the parent ions fragment. All the ions are then ejected from the trap, mass-selected by a second quadrupole filter, and detected by a channeltron. Detecting the number of fragment ions as a function of the laser wavelength gives an electronic photofragment spectrum of the parent molecule. The most abundant UV laser-induced fragment results from the loss of the phenylalanine side chain (i.e., via $C_\alpha-C_\beta$ bond breakage), and we use this fragmentation channel for all measurements. To obtain conformer-selective IR spectra of the cold ions, we tune the UV laser wavelength to a specific transition in the electronic spectrum and introduce an IR pulse from a tunable OPO 200 ns before the UV pulse. This results in depletion of the photofragment signal, which is recorded as a function of IR wavelength.

2.3. Computational Methodology. We generate an initial pool of calculated structures using basin-hopping, as implemented in the Tinker package[64] with the OPLS-AA force field.[16] The energy cutoff was set to 50 kcal/mol, and the number of torsional modes was set to 20. Increasing either of these parameters does not lead to a substantial increase in the number of unique structures generated. The initial pool of structures was then subjected to a conformational clustering procedure from the GROMACS program package,[65,66] and only the lowest-energy representatives of each cluster (cutoff 0.75 Å) were kept.

Collisional cross sections (CCSs) first were calculated using the projection approximation (PA) method[67] implemented in Sigma.[68] Knowing that this method underestimates the collisional cross sections, we selected randomly a set of 20 structures, computed their CCS with the trajectory method (TM[69] in MOBCAL[70]), and used linear regression to find a correspondence between CCSs computed by PA and TM for our system (the coefficient calculated is 1.026). In later stages we calculated the CCSs using the TM method with partial charges extracted from DFT calculations.

All DFT simulations in this work were performed in the all-electron program package FHI-aims based on numeric atom-centered orbital basis sets.[71] Initially, the PBE functional[72] with many-body dispersion correction (MBD)[73,74] was used. The initial relaxations were performed with the "light" species defaults, while for refinement a more accurate "tight" basis was employed. For further improvement of the description of the system, we used the PBE0 functional.[75] These functionals, and the order of increasing accuracy, were proven successful in previous studies.[39,76−78]

For calculations of vibrational spectra, we used scaling factors of 0.948 for PBE0 and 0.978 for PBE. Free energies were estimated based on vibrational frequencies calculated with the PBE functional at 0, 10, and 300 K using harmonic oscillator and rigid rotor approximations.

2.4. Nuclear Magnetic Resonance. The NMR spectra are acquired at room temperature on a Bruker Avance III HD instrument operating at 600 MHz for ^{1}H. We acquire TOCSY, COSY and ROESY (with the mixing time 400 ms) 2D ^{1}H NMR spectra in DMSO and use them to assist interpretation of analogous data obtained in a H_2O:CD_3OH 50:50 mixture, where water suppression is performed with the presaturation sequence. The relative abundances of the conformers are measured by integrating the peak volumes using Mestrelab MNova NMR software.[79]

3. RESULTS

We achieve conformer selectivity in our experiments in two ways: (i) by using ion mobility to separate molecules with different cross sections by their drift time and then recording vibrational spectra of the mobility-selected ions; and (ii) by performing IR-UV double-resonance spectroscopy to obtain vibrational spectra of individual conformers within a mixture.

3.1. Vibrational Spectra of Mobility-Selected Ions. The ion-mobility drift-time distribution of BK[1−5]$^{2+}$ has two well separated peaks, as shown in Figure 2. The first peak has an

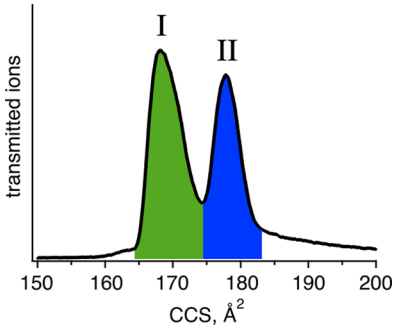

Figure 2. Collisional cross section distribution of BK[1−5]$^{2+}$. The extended conformers (peak II) are kinetically trapped and interconvert to more compact, stable, gas-phase structures (peak I) upon collisional activation.

unresolved shoulder and can be represented as a sum of two Gaussians, one centered at 167 Å^2 and the other at 170 Å^2. The second peak is centered at 178 Å^2, and its width suggests that it may also consist of more than one conformer.

When we select either of the two peaks after they drift through the first part of the drift tube and collisionally activate them, the same arrival-time distribution is produced for both peaks as they drift through the second segment of the drift tube. As shown in Figure 3, this "annealed" distribution consists

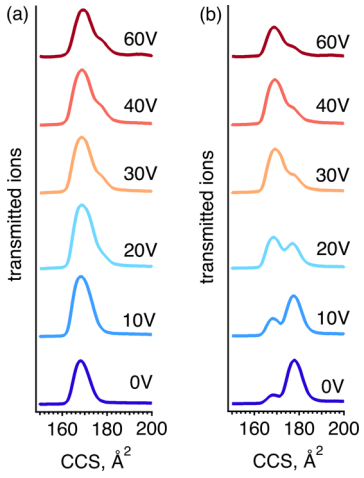

Figure 3. Collisional activation of BK[1−5]$^{2+}$ preselecting (a) peak I and (b) peak II in the drift-time distribution of Figure 2. The color code corresponds to the activation voltage applied.

mainly of peak I with a shoulder around 176 Å^2, slightly more compact than the original extended conformations. We conclude that the structures contained within peak II are kinetically trapped, while peak I represents stable gas-phase structures. This type of behavior has been demonstrated previously for the full bradykinin in the 3+ charge state (BK^{3+}).[80,81]

While ion-mobility spectrometry provides an orientationally averaged CCS of a molecule that reflects its overall shape, vibrational spectroscopy produces a distinct fingerprint that reflects the molecule's precise structure. We thus select both peaks in the ion-mobility distribution and obtain their IR

DOI: 10.1021/jacs.6b04550
J. Am. Chem. Soc. 2016, 138, 9224−9233

spectra via H_2-tagging spectroscopy (Figure 4). We also obtain their vibrational spectra after annealing via collisional activation

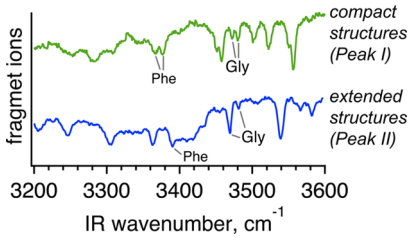

Figure 4. Vibrational spectra of mobility-selected BK[1−5]$^{2+}$. Phenylalanine and glycine NH stretches are assigned by measuring the spectra of ^{15}N-labeled peptides.

(50 V), and we observe that they are practically identical and contain the same bands as the vibrational spectrum of the compact structures (see SI-Figure 2). This confirms that after collisional activation we reach the same quasi-equilibrium gas-phase distribution independent of the starting conformation. This distribution consists of the same conformers as those under the more compact peak in the ion mobility drift-time distribution.

To assign the peaks in the IR spectra to specific vibrational modes, we had two isotopically labeled peptides synthesized by replacing the amide nitrogen of phenylalanine and glycine with ^{15}N. This substitution typically shifts the labeled NH band by ~8 cm^{-1} to the red and allows us to identify the bands that correspond to phenylalanine and glycine NH stretches, which are labeled in Figure 4.

3.2. IR-UV Double Resonance Spectroscopy. One of the most powerful ways to simplify congested spectra of large molecules is to use double-resonance spectroscopy in a cryogenic ion trap.[38] We recorded vibrational spectroscopic signatures of three distinct conformers in our cold, octopole ion trap, shown in Figure 5, and label them A, B, and C. Isotopic labeling allows us to identify the NH stretches of the phenylalanine and glycine residues, which are labeled in Figure 5. Note that the IR spectrum of conformer B is very close to that of conformer A, with the main difference being the frequencies of the phenylalanine NH stretch, which are separated by 27 cm^{-1}. This suggests that these two conformers differ in the rotation of phenylalanine side chain.[82,83]

The spectra in Figure 5 clearly demonstrate that peak I identified by ion mobility consists of conformers A and C. At the same time the spectroscopic differences between spectra of A and B are so small that we cannot exclude presence of small quantities of conformer B. In the CIS instrument that we currently use, ions undergo some collisional activation at the end of the ion funnel. This explains why we observe a set of structures that largely resembles the annealed distribution obtained in our IMS-CIS machine, i.e. mostly the compact structures. Despite the recent finding that H_2-tagging can alter the conformation of small biological molecules,[84] in this case we observe that the spectroscopic features are not detectably shifted when the peptide is tagged with one H_2 molecule.

To summarize the experimental results, the following structures are observed in the gas phase:

- Compact conformations with a CCS in the range of 167−170 Å^2. Analysis of their spectral signatures suggests the presence of conformers A, B and C. B only differs from A in the phenylalanine ring orientation. A third conformer, denoted C, is structurally different from A and B.
- Extended structures with a CCS around 178 Å^2. They are kinetically trapped and upon collisional activation collapse to the more stable compact conformations.

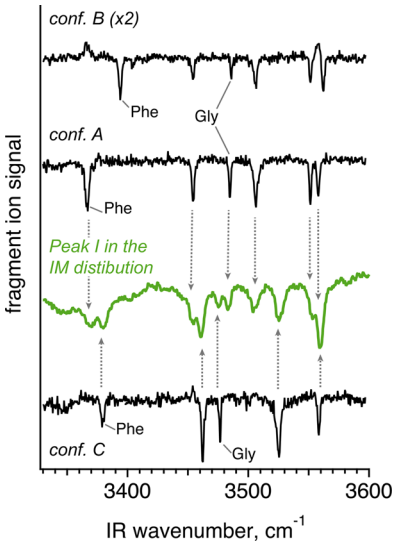

Figure 5. Comparison of vibrational spectra of three conformers (A, B, and C) of BK[1−5]$^{2+}$ obtained in the CIS machine by IR-UV double-resonance together with a vibrational spectrum (in green) of the mobility-selected compact structures recorded in the IMS-CIS machine by H_2-tagging. The low-CCS peak in the arrival-time distribution, accordingly, consists of a mixture of conformers A, C, and, possibly, B. The labels show the NH-stretches that were assigned by measuring the spectra of ^{15}N-labeled peptide.

Previous studies of the full BK sequence suggest that peaks I and II differ by prolyl−peptide bond isomers.[42,85]

3.3. First-Principles Simulations. To determine the structures of the conformers that give rise to the CCS values and infrared spectra that we measure, we have to compare these results with theory. First we must search the massive conformational space for BK[1−5]$^{2+}$ (discretization of the 13 single bonds in 60 degrees steps and of the 4 peptide bonds to *cis* and *trans* states results in roughly 2 × 10^{11} structures to evaluate). We tackle this sampling problem by a two-step approach: (i) a force field-based global screening (basin hopping with Tinker and the OPLS-AA force field), and (ii) subsequent density-functional theory calculations. In order to select the conformers to consider at the higher, first-principles level, we employ experimental constraints, comparing the calculated CCS values and vibrational signatures to their experimental counterparts. The use of experimental constraints is not only a concession to the large conformational search space. Only one of the observed conformers can be the global minimum of the potential-energy surface, while the rest, especially the kinetically trapped species, cannot be determined based on the energy criterion alone.

The initial force field search yields 212 754 conformations that were sorted into 67 546 clusters, the lowest energy representative of which was considered in the following. We first assumed, and later confirmed, that kinetic trapping is a result of the *cis*/*trans* isomerization of the two prolyl−peptide bonds present in BK[1−5]$^{2+}$. All structures were categorized into four groups, *trans*−*trans* (TT), *trans*−*cis* (TC), *cis*−*trans* (CT), and *cis*−*cis* (CC), according to their prolyl−peptide

DOI: 10.1021/jacs.6b04550
J. Am. Chem. Soc. 2016, 138, 9224−9233

bond conformations. We have carried out the following analysis separately for each category so that we are sure to consider structures that are high in energy, such as TT, but that may still be observed experimentally due to kinetic trapping. We selected structures out of these individual sets based on their relative potential energy and calculated CCS. In order to put an emphasis on structures with CCSs that match the experiment, we applied an energy threshold of 30 kcal/mol relative to the lowest energy structure of the same backbone type to structures with CCS values between 165 and 183 Å^2. For structures with a lower or higher CCS, we applied a relative energy threshold of 26 kcal/mol. By this procedure, we selected 4515 structures that were subjected to geometry relaxations using the PBE functional with many-body dispersion correction and "light" computational settings.

3.3.1. Compact Structures: Low-Energy Minima. To find candidates for the equilibrated stable structures of peak I, we rely mainly on the potential energy. First, the clustering procedure was applied to the initial pool of structures, and an energy threshold was used to select the structures to be optimized with "tight" settings. From these, we selected the lowest-energy structures in each proline configuration (TT, TC, CT, or CC, 57 in total) and computed free energies and vibrational spectra in the harmonic approximation using the PBE functional and "tight" settings. Visual inspection of these spectra allowed us to choose the structures that best correspond to those we observed experimentally. We recomputed the spectra of all promising candidates using the PBE0 functional. The resulting spectra and the corresponding structures are shown in Figure 6.

The calculated NH-stretch vibrational frequencies correspond remarkably well to the measured frequencies, including the hydrogen-bonded NH stretches. However, we observe a systematic shift between calculated and experimental frequencies of the free OH stretch vibration. Such a discrepancy can result from (i) the possible incomplete inclusion of electron exchange and correlation and (ii) the use of a single scale factor to globally account for vibrational anharmonicity and nuclear quantum effects.[86] The former issue is resolved by the use of the PBE0 hybrid functional with exact Hartree−Fock exchange. Provided a large data set of computed vs experimentally measured vibrational frequencies is available, the latter could be resolved by finding scaling factors for each vibrational mode by linear regression and subsequently using them for a system with unknown geometry. With this approach, it has been shown that these factors differ between NH and OH stretches.[87] In the absence of such a data set, we use a single scale factor to account for vibrational anharmonicity. In light of this, it is not surprising that the calculated OH vibrational band is shifted from what we measure, since the scale factor is largely determined by the agreement for the more numerous NH stretch bands. Routes toward a correct simulation of the experimental OH stretch peak positions without the need for scaling are known−simulations that fully include anharmonic effects and a quantum mechanical treatment of the nuclear motion. Examples are the multiconfigurational time-dependent Hartree method[88] or the approximate thermostated ring-polymer molecular dynamics method.[89] However, such methodology is not yet straightforwardly applicable to molecules of the size investigated here.

As shown in Figure 6, we were able to assign structures that fit to the spectral signatures that we found in peak I of the CCS distribution. Conformers A and B differ by the orientation of

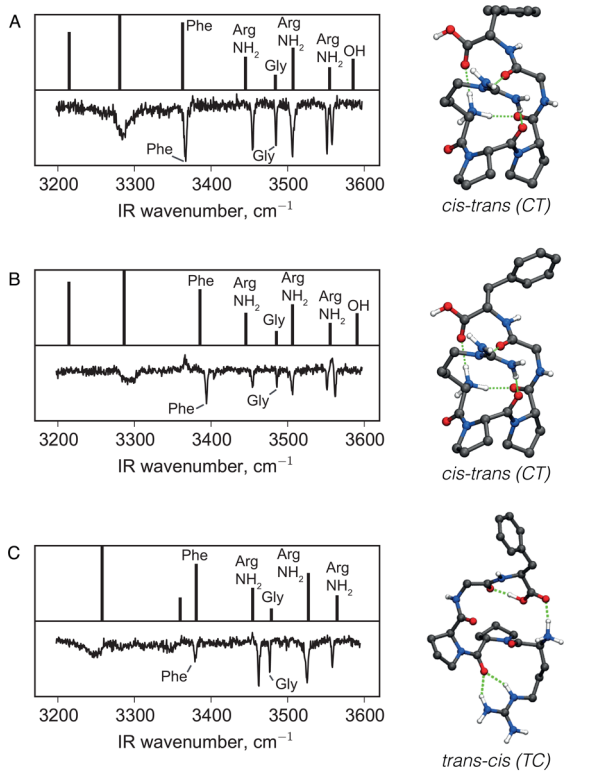

Figure 6. Comparison between calculated and experimental spectra for conformers A, B, and C, forming peak I. The corresponding structures are shown and the conformation of prolyl−peptide bonds is noted for each conformer. The NH stretch vibrations in the experimental spectra are identified via isotopic labeling. For the computed spectra, all relevant local modes are labeled.

the phenylalanine ring, as the experimental data suggest. Conformers A and C have different configurations: in A the prolines are in a *cis*−*trans* configuration, while in C they are *trans*−*cis*. Despite the difference in structure, their calculated CCS values are very close: 169 and 168 Å^2.

We measure ion mobilities at room temperature, and then cool the ions in the cold ion trap. Depending on the rate of cooling, one might expect a certain degree of re-equilibration of the conformational distribution in this process. If the cooling is fast with respect to the isomerization rate between conformers, kinetic trapping can occur, preventing the preferred geometries at 300 K from converting to the low-energy, gas-phase structures at low temperature. In order to gain insight into the dependence of the energy ordering of the different conformations on the temperature of the molecule, we computed the energies of all 57 candidates with the PBE0 functional and then evaluated the free energy for a range of temperatures using a harmonic approximation. Figure 7 shows how the relative energies change within the CT, TC, and CC categories for three cases: pure potential energy, free energy at 10 K, and free energy at 300 K. The importance of the free energy correction can be demonstrated using the example of the conformation that corresponds to the global minimum on the potential-energy surface (PES). It is a very compact CT structure with a CCS of 157 Å^2 and is not observed in the experiment. Indeed, at 300 K, this conformer no longer represents the global minimum.

The energy difference at 300 K between conformer A and the global minimum is within 0.6 meV per atom, which is at the

DOI: 10.1021/jacs.6b04550
J. Am. Chem. Soc. 2016, 138, 9224−9233

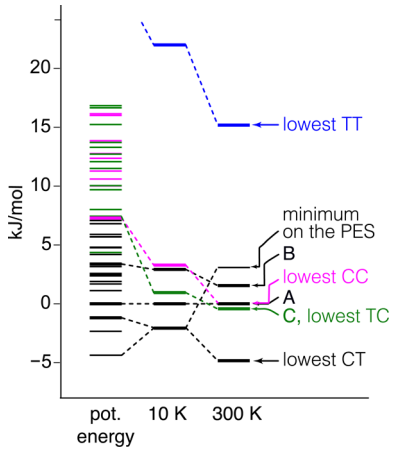

Figure 7. On the left: relative potential energies within CT (black), TC (green), and CC (magenta) configurations. On the right: the change in relative energies of the main conformers for three cases: pure potential energy, free energy at 10 K, and free energy at 300 K. A, B, and C label the experimentally observed conformations. The lowest energy TT structure (blue) is given for a reference. The lowest-energy geometries at 300 K for TC, CT, and CC configurations are labeled as well.

limit of what can be resolved at this level of theory. The global minimum at 300 K (GM 300 K in Table 1) is a CT structure that has the same hydrogen bonding pattern as A and B but which differs from them mainly by rotation of the phenyl ring (see SI-Figure 3). A number of other low-energy structures at 300 K with similar H-bonding patterns and CCSs as A and B have been identified. We speculate that at 300 K the structures of the CT type are close to the global minimum and are rapidly interconverting, while after cooling the ions in the trap we freeze out mainly conformer A and traces of conformer B. The higher the number of similar structures available around the global minimum, the higher is the volume of conformational space corresponding to this basin at 300 K and, accordingly, the higher is the probability to find the molecule there.

Note that conformer C is the lowest-energy structure in the TC category at 300 K. In general, we observe in the experiment the low-energy geometries for CT and TC types but not of the CC type. Further computations of energy barriers between different conformers are needed to fully understand why only a fraction of the available low-energy structures is observed experimentally. It could also lead to a better understanding of the interplay between the collisional cooling rate and the isomerization rate.

3.3.2. Extended Kinetically Trapped Structures. While there is a relatively well-established (though computationally expensive) procedure for searching for the global minimum on a potential energy surface, identifying kinetically trapped conformations is challenging. One cannot rely on the energy criterion, because the kinetically trapped structures lie, by definition, high in energy and are separated from other conformational basins with even higher energy barriers. In this case, experimental constraints play a key role in guiding quantum-chemical calculations. One of them is the CCS. We computed CCSs of all geometries in the initial pool of structures, and as shown in Figure 8a, we considered only those that have a CCS higher than 176 Å^2, which means they fall under peak II in the arrival-time distribution. The energy threshold for a structure to be considered was kept as high as possible: 48 kJ/mol (0.5 eV) from the lowest-energy conformer in each type. We calculated vibrational spectra at the PBE +MBD level for all structures that satisfied these two conditions (135 in total). This enabled a second selection step, apart from the CCS cutoff, based on spectroscopic information:

(1) In the IR spectrum of extended structures (see Figure 4), there are two bands above 3570 cm^{-1}. The only vibration in this molecule that can have such high frequency is OH stretch, suggesting that there at least two conformers under peak II of the drift-time distribution and each of them has a free OH stretch.

(2) In the IR spectrum of peak II there is a unique, intense band at 3538 cm^{-1}, which is too high for a backbone NH vibration and thus corresponds to the side chain of arginine.[83] To decide if this side chain interacts with other parts of the molecule, we compare its spectroscopic signature with those of conformers A, B, and C. Their spectra show that the asymmetric stretch of a *free* η-NH_2 of arginine appears at a frequency higher than 3540 cm^{-1} while the symmetric stretch occurs between 3450 and 3500 cm^{-1}. Since the intense band in the spectrum of peak II (see Figure 4) is slightly lower than this, we conclude that the extended conformers have no free η-NH_2 groups, but a least one weakly interacting with other parts of the molecule.

(3) The free ε-NH stretch of arginine should appear on 3465 cm^{-1}.[90,91] The absence of this band in the spectrum suggests

Table 1. Comparison of the Major Conformers Identified in the Present Study[a]

conf.	prolyl−peptide bond conformation	potential energy, meV[b]	free energy at 10 K, meV[b]	free energy at 300 K, meV[b]	CCS experiment, Å^2	CCS computed, Å^2
GM (pot)	CT	**−45**	−21	32		157
GM (10 K)	CT	12	**−24**	−36		165
GM (300 K)	CT	−12	−21	**−50**		168
A	CT	0	0	0	167, 170	169
B	CT	35	30	16	167, 170	169
C, lowest TC (10 and 300 K)	TC	76	10	−5	167, 170	171
lowest TT (300 K)	TT	280	216	111		175
D	TT	394	322	204	178	177
E	TT	406	336	260	178	176
F	TT	398	322	225	178	177
lowest CC	CC	75	34	1		169

[a]GM denotes the global minimum on the corresponding energy surface. [b]Relative to conformer A.

DOI: 10.1021/jacs.6b04550
J. Am. Chem. Soc. 2016, 138, 9224−9233

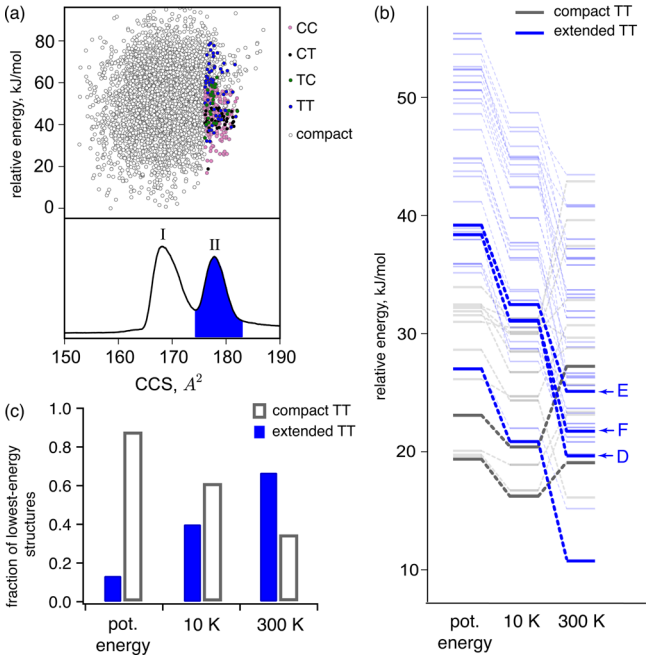

Figure 8. (a) Distribution of relative potential energies of considered conformers as a function of CCS. Those conformations for which the vibrational spectra were computed are shown in color. The rest of the structures are shown in gray. (b) Energy hierarchy for the lowest-energy structures of TT type. The extended structures with CCS higher than 176 Å^2 are shown in blue, and the compact ones in gray. The structures that are found in the experiment and several representative low-energy structures are highlighted to show the general trend. (c) The ratio between compact and extended (CCS higher than 176 Å^2) structures among 15 lowest-energy conformers without and with temperature correction.

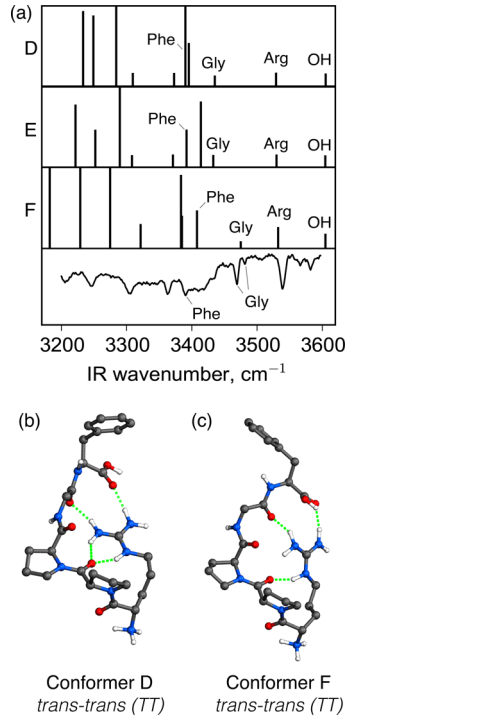

Figure 9. (a) Calculated vibrational spectra of conformers D, E, and F compared to the experimental spectrum of peak II of the arrival-time distribution; (b, c) corresponding structures. Structure of the conformer E is visually almost indistinguishable from the conformer D and is not shown.

that the ε-NH of arginine in all extended conformers is hydrogen bonded.

(4) The strong bands at 3362 and 3303 cm^{-1} are most probably the spectroscopic signature of the free NH_3^+ group or one weakly bound to a phenyl ring.[92]

(5) Based on the comparison with the spectra of conformers A, B, and C, the phenylalanine NH stretch might interact with the phenyl ring, while the NH stretch of glycine appears to be free.

With these considerations we aim to rationalize the comparison between experimental and simulated spectra that otherwise is easily prone to incorrect or imprecise assignment. It is necessary to analyze the spectroscopic features manually and to perform isotopic labeling. After applying the criteria stated above to the simulated spectra and molecular geometries, only structures of type TT remain, meaning that both prolyl peptide bonds are in the *trans* configuration. We recomputed the IR spectra of those structures that satisfy the above criteria with the PBE0 functional, which further improved the agreement between simulated and experimental vibrational spectra (Figure 9a).

Figures 8b and c explain why we observe elongated TT structures in the ion mobility experiment. They are more stable at 300 K than the compact structures, while the latter become more energetically favorable at 10 K. At 300 K, the elongated structures traverse the drift tube, rapidly interconverting between the close minima on the free energy surface. Then they are transferred to the cold ion trap, where the final structure at 10 K results from the interplay between collisional cooling and isomerization. The fact that we observe spectroscopically the elongated structures suggests that some of their features are preserved in the cooling process. Kinetic trapping could occur twice during their transition from solution to our cold ion trap: in the ion source and in the cryogenic ion trap. We observe evidence of some kinetic trapping in both cases.

4. DISCUSSION: OVERVIEW OF THE CONFORMATIONAL SPACE OF BRADYKININ 1−5

Numerous NMR studies of the full bradykinin molecule indicate that in aqueous solution it mainly adopts an all-*trans* conformation,[10−12,14−16] which is consistent with the *trans* bond being slightly more stable than *cis* in polar environments due to its higher dipole moment.[11] Two receptors of bradykinin are known,[93] B1 and B2, and in the complex with the B2 receptor bradykinin is in the all-*trans* form.[13,15] If the medium becomes nonpolar, alternative backbone conformations involving *cis* prolyl peptide bonds are more competitive.[94] The transfer to the gas phase has a similar effect on its structure as the transfer to a nonpolar solvent or interaction with a membrane: the conformations involving the *cis*-configuration of prolyl-peptide bonds become more stable.

We observe the same type of behavior for BK[1−5]$^{2+}$, which acts in vivo as an inhibitor of thrombin. An X-ray structure of the complex demonstrates that all peptide bonds in BK[1−5] remain *trans*.[55] We performed NMR measurements in a CD_3OH/H_2O mixture, which reproduces the solvent used for the ESI experiments. Peaks were assigned using COSY and TOCSY 2D ^{1}H spectra with water suppression, and the assignments are supported by comparison with spectra acquired in DMSO, where no background water signal hinders the cross-

DOI: 10.1021/jacs.6b04550
J. Am. Chem. Soc. 2016, 138, 9224−9233

peaks. No residual secondary structure is identified based on the Hα secondary chemical shifts, which are close to zero for all residues but N-terminal arginine (see SI-Table 1).[95,96] The ROESY 2D ^{1}H NMR spectrum shows that 82% of molecules in a 50:50 water/methanol mixture adopt the *trans*−*trans* configuration (see SI-Figure 1). Three alternative conformers do not have a fully resolved spin system and thus it is difficult to identify them.

Upon electrospraying from the same water/methanol mixture, we observe a kinetically trapped conformational family in which all the bonds remain *trans*. These TT conformers are folded in such a way that the N-terminus of the molecule remains free, while the arginine side chain interacts with the C═O groups of the backbone. The broad ion-mobility peak reflects the disordered behavior in solution. Inside the drift tube at room temperature closely related conformations might be rapidly interconverting, while at 10 K in the conditions of the cold ion trap the structure becomes well-defined. We do not observe the lowest-energy structures of the TT type in the experiment, but rather the ones that lie quite high in energy. This means that the mechanism of kinetic trapping involves not only *cis*−*trans* isomerization, but also H-bond rearrangement, which can have high-energy barriers as well.

Upon collisional activation, TT conformers of BK[1−5]$^{2+}$ (i.e., the extended structures in the IM distribution) convert to TC and CT structures (the compact ones). The relative abundances of these conformers at different degrees of activation observed by cryogenic ion spectroscopy (see SI-Figure 2) suggest that first the TT to TC transition occurs, followed by TT to CT. The alternative pathway via CC conformers is unlikely as we do not find any trace of CC conformers, even though their free energies are close to those of conformers A and C. Further investigation of conversion paths between all types of structures will shed light on this issue. One explanation might be that the barrier height between CC and the rest of the conformational space is significantly higher than between TT and CT or TT and TC, so that the molecule fragments before sampling the CC states.

In all cases except TT, the N-terminus and arginine side chain can both form H-bonds, which stabilize the molecule compared to TT. The external hydrogen bonds have to be substituted by internal ones upon the removal of water. This is why in the gas phase even the lowest-energy TT structure is significantly less stable than TC, CT, and CC (Table 1). These latter three types have compact low-energy structures with CCSs falling within peak I in the drift-time distribution. Low-energy conformers of the TT type tend to be more extended, with CCSs close to peak II in the drift-time distribution. Overall, the calculated CCSs presented in Table 1 agree well with the values that we measure, given that the experimental error is estimated to be around 2 Å^2. The compaction in the gas phase corresponds to the effect observed for BK adhered to the surface of a micelle.[97]

5. CONCLUSION

The combination of ion mobility and cryogenic ion spectroscopy has allowed us to characterize all major conformations of BK[1−5]$^{2+}$ in the gas phase. While only two well-resolved peaks are separated by ion mobility, we show spectroscopically that there are several conformers within each of them. Our calculations reveal that three very different conformational families (*cis*−*trans*, *trans*−*cis*, and *cis*−*cis*) have close free energies and CCSs in the gas phase, and, by combining the experimental spectroscopic information with first-principles simulation data, we were able to assign them. We determine that the lowest-energy gas-phase structures of the peptide feature backbone conformations with the two prolyl-peptide bonds in either *cis*−*trans* or *trans*−*cis* state. Both of them fall within the more compact ion mobility peak at 167−170 Å^2.

Kinetic trapping can occur at different points in the "life cycle" of the ion in our instrument. First, when the ions are initially desolvated in the electrospray, the conformations coming out of solution can be kinetically trapped behind barriers that result from internal hydrogen bonding and separation in *cis*−*trans* states of the prolyl-peptide bonds. Second, if cold-ion spectroscopy is used, kinetic trapping can occur when cooling the molecules. In this case, when the collisional cooling rate is faster than the isomerization rate, the population of conformers that are higher in energy than the global minimum can be trapped behind isomerization barriers.

We have identified the kinetically trapped conformers of BK[1−5]$^{2+}$ as all-*trans*, which is the predominant backbone conformation type in solution. This provides the basis for further gas-phase studies to investigate the isomerization barriers between the prolyl-peptide bond types CC, CT, TC, and TT and to study the extent of microsolvation that is required to render TT more stable than the alternative backbone types. The width of the observed IM peak and the spectroscopic signature of the kinetically trapped conformations suggest a wide variety of structures, which is in agreement with the intrinsic disorder in solution. In stark contrast to this, we have shown that the stable, gas-phase *cis*−*trans* and *trans*−*cis* conformers appear to represent well-defined minima. This is consistent with the notion that disordered peptides collapse to particular secondary structure in nonpolar media such as cell membranes.

■ ASSOCIATED CONTENT

Supporting Information

The Supporting Information is available free of charge on the ACS Publications website at DOI: 10.1021/jacs.6b04550.

ROESY NMR spectrum of bradykinin 1−5 in DMSO and CD_3OH:H_2O solutions; table of secondary chemical shifts of bradykinin 1−5 in CD_3OH:H_2O solution, vibrational spectrum of annealed conformational distribution of bradykinin 1−5; structure of lowest-energy conformer of bradykinin 1−5 in the gas phase (PDF)

■ AUTHOR INFORMATION

Corresponding Authors

*Thomas.Rizzo@epfl.ch

*baldauf@fhi-berlin.mpg.de

Present Address

‖A.M.: Lawrence Berkeley National Laboratory, Earth Sciences Division, 1 Cyclotron Rd., MS74R316C, Berkeley, California 94720, USA.

Notes

The authors declare no competing financial interest.

■ ACKNOWLEDGMENTS

We are grateful to the EPFL, the Swiss National Science Foundation (Grant Number 200020_152804) and the joint EPFL-Max Planck Center for Molecular Nanotechnology for the financial support of this work. The authors also thank Dr. Pascal Mieville and Dr. Luc Patiny for the NMR data. CB

DOI: 10.1021/jacs.6b04550
J. Am. Chem. Soc. 2016, 138, 9224−9233

thanks Dr. Mariana Rossi for sharing her knowledge about theoretical vibrational spectroscopy and Prof. Matthias Scheffler for his continuous support.

REFERENCES

(1) Uversky, V. N.; Dunker, A. K. *Biochim. Biophys. Acta, Proteins Proteomics* **2010**, *1804*, 1231−1264.
(2) Turoverov, K. K.; Kuznetsova, I. M.; Uversky, V. N. *Prog. Biophys. Mol. Biol.* **2010**, *102*, 73−84.
(3) Kaltashov, I. A.; Eyles, S. J. *Mass Spectrometry in Biophysics: Conformation and Dynamics of Biomolecules*; John Wiley & Sons: Hoboken, NJ, 2005; pp 45−86.
(4) Mittag, T.; Forman-Kay, J. D. *Curr. Opin. Struct. Biol.* **2007**, *17*, 3−14.
(5) Jensen, M. R.; Markwick, P. R.; Meier, S.; Griesinger, C.; Zweckstetter, M.; Grzesiek, S.; Bernado, P.; Blackledge, M. *Structure* **2009**, *17*, 1169−1185.
(6) Henzler-Wildman, K.; Kern, D. *Nature* **2007**, *450*, 964−972.
(7) Gibbs, E. B.; Showalter, S. A. *Biochemistry* **2015**, *54*, 1314−1326.
(8) Dunker, A. K.; Silman, I.; Uversky, V. N.; Sussman, J. L. *Curr. Opin. Struct. Biol.* **2008**, *18*, 756−764.
(9) Regoli, D.; Barabe, J. *Pharmacol. Rev.* **1980**, *32*, 1−46.
(10) Richard, T.; Vergé, S.; Berké, B.; Vercauteren, J.; Monti, J. P. *J. Biomol. Struct. Dyn.* **2001**, *18*, 627−637.
(11) Young, J. K.; Hicks, R. P. *Biopolymers* **1994**, *34*, 611−623.
(12) Gaggelli, E.; D'Amelio, N.; Maccotta, A.; Valensin, G. *Eur. J. Biochem.* **1999**, *262*, 268−276.
(13) Lopez, J. J.; Shukla, A. K.; Reinhart, C.; Schwalbe, H.; Michel, H.; Glaubitz, C. *Angew. Chem., Int. Ed.* **2008**, *47*, 1668−1671.
(14) Glover, M. S.; Bellinger, E. P.; Radivojac, P.; Clemmer, D. E. *Anal. Chem.* **2015**, *87*, 8466−8472.
(15) Ottleben, H.; Haasemann, M.; Ramachandran, R.; Gorlach, M.; MullerEsterl, W.; Brown, L. R. *Eur. J. Biochem.* **1997**, *244*, 471−478.
(16) Kaminski, G. A.; Friesner, R. A.; Tirado-Rives, J.; Jorgensen, W. L. *J. Phys. Chem. B* **2001**, *105*, 6474−6487.
(17) Richard, T.; Delaunay, J. C.; Mérillon, J. M.; Monti, J. P. *J. Biomol. Struct. Dyn.* **2003**, *21*, 379−385.
(18) Bonechi, C.; Ristori, S.; Martini, G.; Martini, S.; Rossi, C. *Biochim. Biophys. Acta, Biomembr.* **2009**, *1788*, 708−716.
(19) Gothel, S. F.; Marahiel, M. A. *Cell. Mol. Life Sci.* **1999**, *55*, 423−436.
(20) Fanghänel, J. r.; Fischer, G. *Front. Biosci., Landmark Ed.* **2004**, *9*, 3453−3478.
(21) Nigro, P.; Pompilio, G.; Capogrossi, M. C. *Cell Death Dis.* **2013**, *4*, e888.
(22) Satoh, K.; Matoba, T.; Suzuki, J.; O'Dell, M. R.; Nigro, P.; Cui, Z.; Mohan, A.; Pan, S.; Li, L.; Jin, Z.-G.; Yan, C.; Abe, J.-i.; Berk, B. C. *Circulation* **2008**, *117*, 3088−3098.
(23) Zoldák, G.; Aumüller, T.; Lücke, C.; Hritz, J.; Oostenbrink, C.; Fischer, G.; Schmid, F. X. *Biochemistry* **2009**, *48*, 10423−10436.
(24) Kunz, C.; Jahreis, G.; Gunther, R.; Berger, S.; Fischer, G.; Hofmann, H. J. *J. Pept. Sci.* **2012**, *18*, 400−404.
(25) Baldauf, C.; Pagel, K.; Warnke, S.; von Helden, G.; Koksch, B.; Blum, V.; Scheffler, M. *Chem. - Eur. J.* **2013**, *19*, 11224−11234.
(26) Warnke, S.; Baldauf, C.; Bowers, M. T.; Pagel, K.; von Helden, G. *J. Am. Chem. Soc.* **2014**, *136*, 10308−10314.
(27) Valiaev, A.; Lim, D. W.; Oas, T. G.; Chilkoti, A.; Zauscher, S. *J. Am. Chem. Soc.* **2007**, *129*, 6491−6497.
(28) Zhang, X.; Halvorsen, K.; Zhang, C.-Z.; Wong, W. P.; Springer, T. A. *Science* **2009**, *324*, 1330−1334.
(29) Chen, J.; Edwards, S. A.; Gräter, F.; Baldauf, C. *J. Phys. Chem. B* **2012**, *116*, 9346−9351.
(30) Beveridge, R.; Phillips, A. S.; Denbigh, L.; Saleem, H. M.; MacPhee, C. E.; Barran, P. E. *Proteomics* **2015**, *15*, 2872−2883.
(31) Buchberger, A.; Yu, Q.; Li, L. *Annu. Rev. Anal. Chem.* **2015**, *8*, 485−509.
(32) Schennach, M.; Breuker, K. *J. Am. Soc. Mass Spectrom.* **2015**, *26*, 1059−1067.
(33) Boeri Erba, E.; Petosa, C. *Protein Sci.* **2015**, *24*, 1176−1192.
(34) Konermann, L.; Vahidi, S.; Sowole, M. A. *Anal. Chem.* **2014**, *86*, 213−232.
(35) Wyttenbach, T.; Pierson, N. A.; Clemmer, D. E.; Bowers, M. T. *Annu. Rev. Phys. Chem.* **2014**, *65*, 175−196.
(36) Stedwell, C. N.; Galindo, J. F.; Roitberg, A. E.; Polfer, N. C. *Annu. Rev. Anal. Chem.* **2013**, *6*, 267−285.
(37) Balasubramaniam, D.; Komives, E. *Biochim. Biophys. Acta, Proteins Proteomics* **2013**, *1834*, 1202−1209.
(38) Rizzo, T. R.; Stearns, J.; Boyarkin, O. V. *Int. Rev. Phys. Chem.* **2009**, *28*, 481−515.
(39) Baldauf, C.; Rossi, M. *J. Phys.: Condens. Matter* **2015**, *27*, 493002.
(40) Wyttenbach, T.; von Helden, G.; Bowers, M. T. *J. Am. Chem. Soc.* **1996**, *118*, 8355−8364.
(41) Pierson, N. A.; Chen, L.; Valentine, S. J.; Russell, D. H.; Clemmer, D. E. *J. Am. Chem. Soc.* **2011**, *133*, 13810−13813.
(42) Pierson, N. A.; Chen, L.; Russell, D. H.; Clemmer, D. E. *J. Am. Chem. Soc.* **2013**, *135*, 3186−3192.
(43) Bohrer, B. C.; Merenbloom, S. I.; Koeniger, S. L.; Hilderbrand, A. E.; Clemmer, D. E. *Annu. Rev. Anal. Chem.* **2008**, *1*, 293−327.
(44) Chen, S. H.; Russell, D. H. *J. Am. Soc. Mass Spectrom.* **2015**, *26*, 1433−1443.
(45) Papadopoulos, G.; Svendsen, A.; Boyarkin, O. V.; Rizzo, T. R. *J. Am. Soc. Mass Spectrom.* **2012**, *23*, 1173−1181.
(46) Pierson, N. A.; Clemmer, D. E. *Int. J. Mass Spectrom.* **2015**, *377*, 646−654.
(47) Silveira, J. A.; Fort, K. L.; Kim, D.; Servage, K. A.; Pierson, N. A.; Clemmer, D. E.; Russell, D. H. *J. Am. Chem. Soc.* **2013**, *135*, 19147−19153.
(48) van der Spoel, D.; Marklund, E. G.; Larsson, D. S. D.; Caleman, C. *Macromol. Biosci.* **2011**, *11*, 50−59.
(49) Breuker, K.; McLafferty, F. W. *Proc. Natl. Acad. Sci. U. S. A.* **2008**, *105*, 18145−18152.
(50) Breuker, K.; Brüschweiler, S.; Tollinger, M. *Angew. Chem., Int. Ed.* **2011**, *50*, 873−877.
(51) Shelimov, K. B.; Jarrold, M. F. *J. Am. Chem. Soc.* **1997**, *119*, 2987−2994.
(52) Kjaergaard, M. *Intrinsically Disord. Proteins* **2015**, *3*, 1−7.
(53) Murphey, L. J.; Hatchey, D. L.; Oates, J. A.; Morrow, J. D.; Brown, N. J. *J. Pharmacol. Exp. Ther.* **2000**, *294*, 263−269.
(54) Morinelli, T. A.; Webb, J. G.; Jaffa, A. A.; Privitera, P. J.; Margolius, H. S. *J. Pharmacol. Exp. Ther.* **2001**, *296*, 71−76.
(55) Hasan, A. A. K.; Warnock, M.; Nieman, M.; Srikanth, S.; Mahdi, F.; Krishnan, R.; Tulinsky, A.; Schmaier, A. H. *Am. J. Physiol. Heart Circ. Physiol.* **2003**, *285*, 183−193.
(56) Nieman, M. T.; Pagan-Ramos, E.; Warnock, M.; Krijanovski, Y.; Hasan, A. A. K.; Schmaier, A. H. *FEBS Lett.* **2005**, *579*, 25−29.
(57) Sawyer, H. a.; Marini, J. T.; Stone, E. G.; Ruotolo, B. T.; Gillig, K. J.; Russell, D. H. *J. Am. Soc. Mass Spectrom.* **2005**, *16*, 893−905.
(58) Svendsen, A.; Lorenz, U. J.; Boyarkin, O. V.; Rizzo, T. R. *Rev. Sci. Instrum.* **2010**, *81*, 073107.
(59) Masson, A.; Kamrath, M. Z.; Perez, M. A.; Glover, M. S.; Rothlisberger, U.; Clemmer, D. E.; Rizzo, T. R. *J. Am. Soc. Mass Spectrom.* **2015**, *26*, 1444−1454.
(60) Koeniger, S. L.; Merenbloom, S. I.; Valentine, S. J.; Jarrold, M. F.; Udseth, H. R.; Smith, R. D.; Clemmer, D. E. *Anal. Chem.* **2006**, *78*, 4161−4174.
(61) Kamrath, M. Z.; Garand, E.; Jordan, P. A.; Leavitt, C. M.; Wolk, A. B.; Van Stipdonk, M. J.; Miller, S. J.; Johnson, M. A. *J. Am. Chem. Soc.* **2011**, *133*, 6440−6448.
(62) Nagornova, N. S.; Rizzo, T. R.; Boyarkin, O. V. *Angew. Chem., Int. Ed.* **2013**, *52*, 6002−6005.
(63) Kelly, R. T.; Tolmachev, A. V.; Page, J. S.; Tang, K.; Smith, R. D. *Mass Spectrom. Rev.* **2010**, *29*, 294−312.
(64) Pappu, R. V.; Hart, R. K.; Ponder, J. W. *J. Phys. Chem. B* **1998**, *102*, 9725−9742.
(65) Van Der Spoel, D.; Lindahl, E.; Hess, B.; Groenhof, G.; Mark, A. E.; Berendsen, H. J. C. *J. Comput. Chem.* **2005**, *26*, 1701−1718.

DOI: 10.1021/jacs.6b04550
J. Am. Chem. Soc. 2016, 138, 9224−9233

(66) Hess, B.; Kutzner, C.; van der Spoel, D.; Lindahl, E. *J. Chem. Theory Comput.* **2008**, *4*, 435−447.
(67) Wyttenbach, T.; Helden, G.; Batka, J. J.; Carlat, D.; Bowers, M. T. *J. Am. Soc. Mass Spectrom.* **1997**, *8*, 275−282.
(68) https://labs.chem.ucsb.edu/bowers/michael/theory_analysis/cross-sections/sigma.shtml.
(69) Mesleh, M. F.; Hunter, J. M.; Shvartsburg, A. A.; Schatz, G. C.; Jarrold, M. F. *J. Phys. Chem.* **1996**, *100*, 16082−16086.
(70) http://www.indiana.edu/~nano/software/.
(71) Blum, V.; Gehrke, R.; Hanke, F.; Havu, P.; Havu, V.; Ren, X.; Reuter, K.; Scheffler, M. *Comput. Phys. Commun.* **2009**, *180*, 2175−2196.
(72) Perdew, J. P.; Burke, K.; Ernzerhof, M. *Phys. Rev. Lett.* **1996**, *77*, 3865−3868.
(73) DiStasio, R. A.; von Lilienfeld, O. A.; Tkatchenko, A. *Proc. Natl. Acad. Sci. U. S. A.* **2012**, *109*, 14791−14795.
(74) Tkatchenko, A.; Distasio, R. A.; Car, R.; Scheffler, M. *Phys. Rev. Lett.* **2012**, *108*, 236402.
(75) Adamo, C.; Barone, V. *J. Chem. Phys.* **1999**, *110*, 6158−6158.
(76) Rossi, M.; Chutia, S.; Scheffler, M.; Blum, V. *J. Phys. Chem. A* **2014**, *118*, 7349−7359.
(77) Schubert, F.; Pagel, K.; Rossi, M.; Warnke, S.; Salwiczek, M.; Koksch, B.; von Helden, G.; Blum, V.; Baldauf, C.; Scheffler, M. *Phys. Chem. Chem. Phys.* **2015**, *17*, 5376−5385.
(78) Schubert, F.; Rossi, M.; Baldauf, C.; Pagel, K.; Warnke, S.; von Helden, G.; Filsinger, F.; Kupser, P.; Meijer, G.; Salwiczek, M.; Koksch, B.; Scheffler, M.; Blum, V. *Phys. Chem. Chem. Phys.* **2015**, *17*, 7373−7385.
(79) http://mestrelab.com/software/mnova/nmr/.
(80) Pierson, N. A.; Valentine, S. J.; Clemmer, D. E. *J. Phys. Chem. B* **2010**, *114*, 7777−7783.
(81) Voronina, L.; Rizzo, T. R. *Phys. Chem. Chem. Phys.* **2015**, *17*, 25828−25836.
(82) Stearns, J.; Seaiby, C.; Boyarkin, O. V.; Rizzo, T. R. *Phys. Chem. Chem. Phys.* **2009**, *11*, 125−132.
(83) Zabuga, A. V.; Rizzo, T. R. *J. Phys. Chem. Lett.* **2015**, *6*, 1504−1508.
(84) Masson, A.; Williams, E. R.; Rizzo, T. R. *J. Chem. Phys.* **2015**, *143*, 104313.
(85) Morrison, L. J.; Wysocki, V. H. *Int. J. Mass Spectrom.* **2015**, *391*, 2−10.
(86) Scott, A. P.; Radom, L. *J. Phys. Chem.* **1996**, *100*, 16502−16513.
(87) Bouteiller, Y.; Gillet, J.-C.; Grégoire, G.; Schermann, J. P. *J. Phys. Chem. A* **2008**, *112*, 11656−11660.
(88) Vendrell, O.; Gatti, F.; Meyer, H.-D. *J. Chem. Phys.* **2007**, *127*, 184303.
(89) Rossi, M.; Ceriotti, M.; Manolopoulos, D. E. *J. Chem. Phys.* **2014**, *140*, 234116.
(90) Bush, M. F.; O'Brien, J. T.; Prell, J. S.; Saykally, R. J.; Williams, E. R. *J. Am. Chem. Soc.* **2007**, *129*, 1612−1622.
(91) Polfer, N. C.; Oomens, J. *Mass Spectrom. Rev.* **2009**, *28*, 468−494.
(92) Chiavarino, B.; Crestoni, M. E.; Schutz, M.; Bouchet, A.; Piccirillo, S.; Steinmetz, V.; Dopfer, O.; Fornarini, S. *J. Phys. Chem. A* **2014**, *118*, 7130−7138.
(93) Takano, M.; Matsuyama, S. *Eur. J. Pharmacol.* **2014**, *732*, 169−172.
(94) Cann, J. R.; Liu, X.; Stewart, J. M.; Gera, L.; Kotovych, G. *Biopolymers* **1994**, *34*, 869−878.
(95) Eliezer, D. In *Methods in Molecular Biology: Protein Folding Protocols*; Bai, Y., Nussinov, R., Eds.; Humana Press Inc.: Totowa, NJ, 2007; Vol. *350*, pp 49−67.
(96) Wishart, D. S.; Bigam, C. G.; Holm, A.; Hodges, R. S.; Sykes, B. D. *J. Biomol. NMR* **1995**, *5*, 67−81.
(97) Montaldi, L. R.; Berardi, M.; Souza, E. S.; Juliano, L.; Ito, A. S. *J. Fluoresc.* **2012**, *22*, 1151−1158.

DOI: 10.1021/jacs.6b04550
J. Am. Chem. Soc. 2016, 138, 9224−9233